2000

A Comprehensive Model of Scroll Compressors Part II: Overall Scroll Compressor Modeling

Y. Chen
Purdue University

N. P. Halm
Purdue University

E. A. Groll
Purdue University

J. E. Braun
Purdue University

A Comprehensive Model of Scroll Compressors
Part II: Overall Scroll Compressor Modeling

Yu Chen **Nils P. Halm**
Eckhard A. Groll **James E. Braun**
School of Mechanical Engineering,
Purdue University, West Lafayette, IN 47907

This paper presents the development of a comprehensive scroll compressor model which combines a detailed compression process model (Chen et al, 2000) and an overall compressor model. In the overall model, compressor components are analyzed in terms of nine different elements. Steady state energy balance equations are established applying the lumped capacitance method. In combination with the detailed compression process model, these equations were implemented into computer code and solved iteratively. In this way, the temperature and pressure of the refrigerant in different compressor chambers, the temperature distributions in the scroll wraps, and the temperatures of the other compressor elements can be obtained. Thereafter, power consumption and efficiency of the compressor can be calculated.

Tests were used to verify the overall model on a macroscopic basis. Using the simulation program based on the overall compressor model, a parametric study of the scroll compressor was performed, and the effects of internal leakage and heat transfer losses were investigated and some preliminary results were obtained. These results indicate that the comprehensive scroll compressor model is capable of predicting real compressor behavior and useful to the design and optimization of scroll compressors.

INTRODUCTION

This paper presents the development of an overall compressor model and combines it with a detailed compression process model (Chen et al, 2000) into a comprehensive scroll compressor model.

The compressor investigated is a 13.42 cc horizontal scroll compressor, which utilizes a high pressure shell, i.e. the entire compressor shell is under discharge pressure. The refrigerant R22 is drawn into the suction chamber in the pump assembly through a suction pipe that leads through the compressor head. The refrigerant is compressed in the pump assembly and discharged through the discharged opening into the compressor head, where it flows over the suction pipe. From the compressor head the compressed gas flows through small holes in the side of the pump assembly, which is three-point welded into the compressor shell, over the compressor motor towards the compressor outlet. The motor is mounted onto the compressor shaft, driving the orbiting scroll, which is prevented from spinning by an oldham coupling in the pump assembly. A trochoidal pump supplies oil to the bearing pump assembly through a drilling in the shaft. Since the compressor is of a horizontal type, part of the pump assembly and the motor are located in the oil sump.

OVERALL ENERGY BALANCE

In order to determine the heat transfer rate between the gas and certain elements of the scroll compressor, temperatures of these elements have to be known. An overall energy balance for the compressor is established.

Lumped Capacitance Method

The scroll compressor and its components are split up into different 'lumped capacitance' elements which are associated with a 'lump temperature'. An equivalent electrical circuit for the thermal masses and their corresponding thermal resistances is shown in figure 1. For the investigated compressor, its components are divided into nine different lumps: the compressor shell, the motor rotor, the motor stator, the compressor oil, the refrigerant, the aluminum scroll, the steel scroll, the suction pipe on the outside of the compressor (pipe 1), the suction pipe on the inside of the compressor (pipe 2).

Steady-state energy balances lead to the following equations for the nine different elements:

$$T_{gas}: \qquad \dot{m}(h_{gas}-h_{dis}) = \frac{T_{pipe2}-T_{gas}}{R_{13}} + \frac{T_{rotor}-T_{gas}}{R_{16}} + \frac{T_{stat}-T_{gas}}{R_{17}} \tag{1}$$

$$T_{pipe1}: \quad 0 = \frac{T_{amb} - T_{pipe1}}{R_{210}} + \dot{Q}_{pipe1} \tag{2}$$

$$T_{pipe2}: \quad 0 = \frac{T_{gas} - T_{pipe2}}{R_{13}} + \dot{Q}_{pipe2} \tag{3}$$

$$T_{steel}: \quad 0 = \frac{T_{alum} - T_{steel}}{R_{45}} + \frac{T_{shell} - T_{steel}}{R_{48}} + \dot{Q}_{average\_steel} + \dot{Q}_{friction\_steel} \tag{4}$$

$$T_{alum}: \quad 0 = \frac{T_{steel} - T_{alum}}{R_{45}} + \dot{Q}_{average\_alum} + \dot{Q}_{friction\_alum} \tag{5}$$

$$T_{rot}: \quad 0 = \frac{T_{gas} - T_{rot}}{R_{16}} + \frac{T_{stat} - T_{rot}}{R_{67}} + \dot{Q}_{friction\_rot} \tag{6}$$

$$T_{stat}: \quad 0 = \frac{T_{gas} - T_{stat}}{R_{17}} + \frac{T_{rot} - T_{stat}}{R_{67}} + \frac{T_{shell} - T_{stat}}{R_{78}} + \dot{Q}_{friction\_stat} + \dot{Q}_{motor} \tag{7}$$

$$T_{shell}: \quad 0 = \frac{T_{steel} - T_{shell}}{R_{48}} + \frac{T_{stat} - T_{shell}}{R_{78}} + \frac{T_{oil} - T_{shell}}{R_{89}} + \frac{T_{amb} - T_{shell}}{R_{810}} \tag{8}$$

$$T_{oil}: \quad 0 = \frac{T_{shell} - T_{oil}}{R_{89}} + \dot{Q}_{friction\_oil} \tag{9}$$

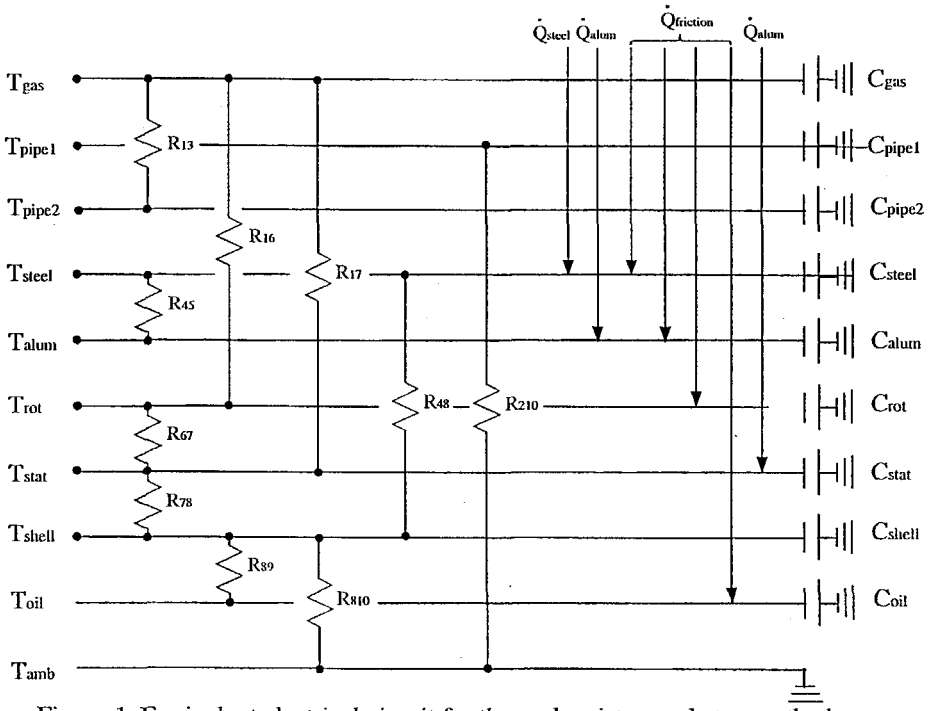

Figure 1 Equivalent electrical circuit for thermal resistances between the lumps

From equation (1), it should be noted that the refrigerant, after being discharged from the pump assembly into the compressor shell, is heated additionally by the different compressor elements, since losses in the motor and the friction between the compressor moving elements are dissipated in the form of thermal energy.

Compression Process Modeling

The compression process modeling is embedded into the energy balances and is described by Chen et al (2000). The unknowns $\dot{m}$, h_{dis}, $\dot{Q}_{pipe1}$, $\dot{Q}_{pipe2}$, $\dot{Q}_{average\_steel}$, $\dot{Q}_{average\_alum}$ in equations (1) to (5), and the compression work $\dot{W}_{compression}$ can be determined by solving the compression process model.

Mechanical/Motor Losses and Compressor Efficiencies

Both motor losses and mechanical losses are combined by defining one efficiency, $\eta_{motor-mechanical}$, as follows:

$$\eta_{motor-mechanical} = \frac{\dot{W}_{compression}}{P} \tag{10}$$

Thus, the power input P to the compressor can be calculated as the compression work over the motor-mechanical efficiency. This efficiency can be calculated by regression based on the performance testing results of the scroll compressor and using the following form of equation:

$$\eta_{motor-mechanical} = a_1 + a_2 \ln\frac{P_{dis}}{P_{suc}} + a_3 \dot{W}_{compression} + a_4 \dot{W}_{compression} \ln\frac{P_{dis}}{P_{suc}} \tag{11}$$

Defining $\dot{Q}_{loss}$ to be the heat transfer within the compressor elements due to both motor losses and mechanical losses, the following energy balance can be established:

$$P = \dot{W}_{compression} + \dot{Q}_{loss} \tag{12}$$

For the aim of a frictional analysis, Hayano reported (1988) a loss distribution of 70% motor and 30% mechanical losses. Therefore,

$$\dot{Q}_{friction} = 0.3\,\dot{Q}_{loss} \tag{13}$$

$$\dot{Q}_{motor} = 0.7\,\dot{Q}_{loss} \tag{14}$$

It is assumed that all motor losses occur in the motor stator.

The heat transfer to various compressor elements due to frictional losses is weighted so that the aluminum and steel scroll, the motor rotor and stator counts for 10% each of the total heat transfer due to the frictional losses, respectively, while oil counts the other 60% (Halm, 1997).

Thermodynamic Relations

Since two independent intensive properties can describe a thermodynamic state, T_{gas} and h_{suc} can be calculated as a function of the other two thermodynamic properties by using the state equation of the refrigerant:

$$T_{gas} = T(h_{gas}, P_{dis}) \tag{15}$$

$$h_{suc} = h(T_{suc}, P_{suc}) \tag{16}$$

Solving the Equations for the Overall Compressor Model

So far, 28 equations (equation (1) to (16) plus 7 equations from the coupled compression process model and 5 equations by weighing the frictional losses) have been established and there are 28 unknowns in these equations ($\dot{m}$, h_{gas}, h_{dis}, T_{gas}, T_{pipe1}, T_{pipe2}, T_{steel}, T_{alum}, T_{rot}, T_{stat}, T_{shell}, T_{oil}, $\dot{Q}_{average\_steel}$, $\dot{Q}_{average\_alum}$, $\dot{Q}_{friction\_steel}$, $\dot{Q}_{friction\_alum}$, $\dot{Q}_{friction\_rot}$, $\dot{Q}_{friction\_stat}$, $\dot{Q}_{friction\_oil}$, $\dot{Q}_{motor}$, $\dot{Q}_{pipe1}$, $\dot{Q}_{pipe2}$, P, $\eta_{motor-mechanical}$, $\dot{W}_{comp}$, $\dot{Q}_{loss}$, h_{suc}, $\dot{Q}_{friction}$). Therefore, these equations are closed and can be solved. Since equation (2) to (10) are non-linear equations and coupled, an iteration method needs to be used to solve the system of non-linear equations.

In order to simplify this system of non-linear equations, an energy balance equation for the entire compressor is used and the number of the non-linear equations can be reduced by one. The global energy balance for the entire compressor yields (Halm, 1997):

$$P = \dot{m}\,(h_{gas} - h_{suc}) + \dot{Q}_{ambient} \tag{17}$$

The heat transfer to the ambient $\dot{Q}_{ambient}$ is

$$\dot{Q}_{ambient} = \frac{T_{pipe1} - T_{amb}}{R_{210}} + \frac{T_{shell} - T_{amb}}{R_{810}} \tag{18}$$

Equation (1) and equation (17) are dependent and one of these two equations should be used. Since by using equation (17), the system of non-linear equations (equation (1) to equation (9)) can be simplified (the number of the non-linear equations can be reduced by one), equation (17) is used in place of equation (1) to speed up the calculations.

The Newton-Raphson method as described by Conte and DeBoor (1980) can be used to solve the non-linear system of equations for the overall energy balance iteratively. It should be noted that since the overall energy balance and the compression process model are coupled to each other, the overall compressor model must call the compression process model at each iteration.

Determination of Thermal Resistances in the Overall Energy Balance

For the evaluation of the temperatures of the different compressor elements as defined in the overall energy balance, the thermal resistances can be determined by employing a least square method to fit the resistances to measured data of the element temperatures. Up to this point, internal measurements of the scroll compressor have not been taken. As a first step, a representative temperature distribution was assumed for a single operating point. The discharge temperature of the gas and the shell temperature were measured and did not need to be assumed. The temperatures of other elements were then chosen based upon the expected directions for heat transfer and reasonable guesses: $T_{gas} = 354\,K$, $T_{pipe1} = 285\,K$, $T_{pipe2} = 300\,K$, $T_{steel} = 319\,K$, $T_{alum} = 318\,K$, $T_{rot} = 355\,K$, $T_{stat} = 360\,K$, $T_{shell} = 354\,K$, $T_{oil} = 355\,K$. Therefore, the nine different thermal resistances can be calculated analytically for the assumed temperature distribution.

EXPERIMENTAL INVESTIGATION

In order to validate the scroll compressor model, experimental investigations have been performed. For this purpose, a compressor load stand was designed and built, which allows the measurement of compressor performance characteristics such as power consumption, discharge pressure, and suction temperature. The compressor load stand was designed using hot gas bypass for control.

MODEL VERIFICATION

Using the compressor load stand, measurements of the compressor's mass flow rate, power input and discharge temperature have been performed. The measurements were taken for nine different operating conditions. All measurements were taken for a driving frequency of 60 Hz and a superheat of 10 °C. The operating pressures and temperatures were fluctuating around their set point. Therefore, the set point pressures and temperatures have an uncertainty of ±5 kPa for the pressures and ±1 °C for the suction temperature. The measured mass flow rate, power input and discharge temperature also displayed a fluctuating behavior, and their uncertainties are ±1 kg/h for the mass flow rate, ±1 °C for the discharge temperature and ±20 W for the power input.

Comparison of the measured and the calculated data for the nine operating points are presented in figure 2 to 4. It can be seen that the trend of variation of mass flow rate, power input and discharge temperature with evaporation temperature (defined as saturation temperature of the suction pressure) and with condensing temperature (defined as saturation temperature of the discharge pressure) is predicted very well by the model in figures 2, 3 and 4. The discharge temperature T_{gas} of the refrigerant was calculated by equation (15) and the enthalpy of the discharged refrigerant h_{gas} was calculated by equation (17). Therefore, the accuracy of the predicted discharge temperature is dependent on the accuracy of the predicted mass flow rate and power input. It can be seen that when the mass flow rate is overpredicted, the discharge temperature tends to be underpredicted or vice versa.

Since the calculated data is very close to the measured data, it can be concluded that the compressor model is capable of predicting real compressor behavior.

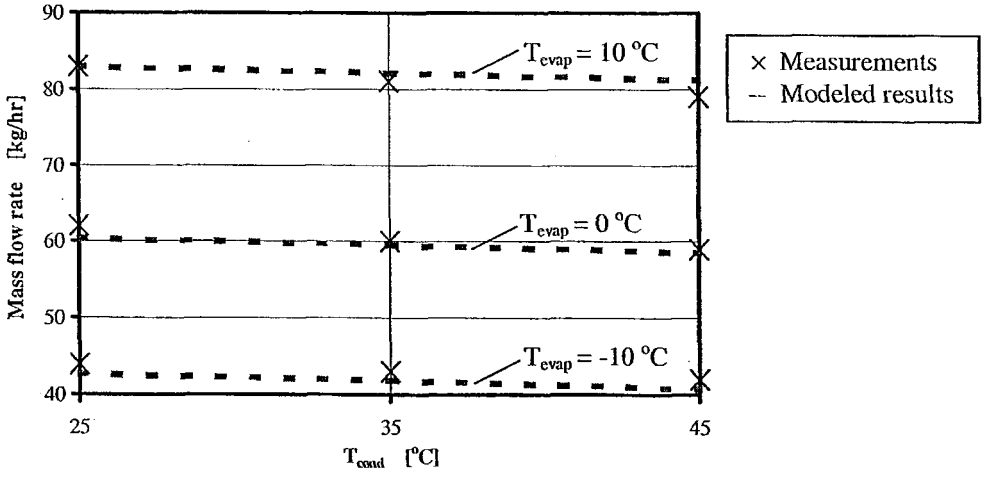

Figure 2 Verification of the mass flow rate

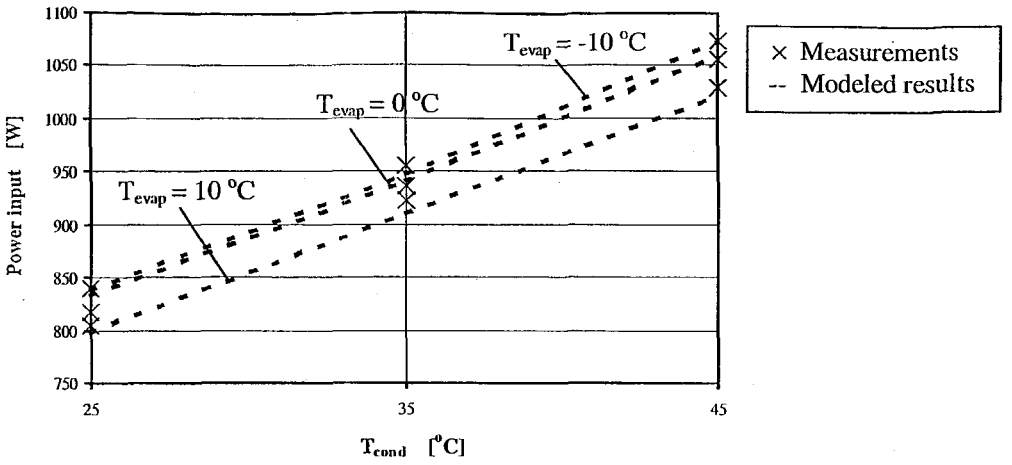

Figure 3 Verification of the power input

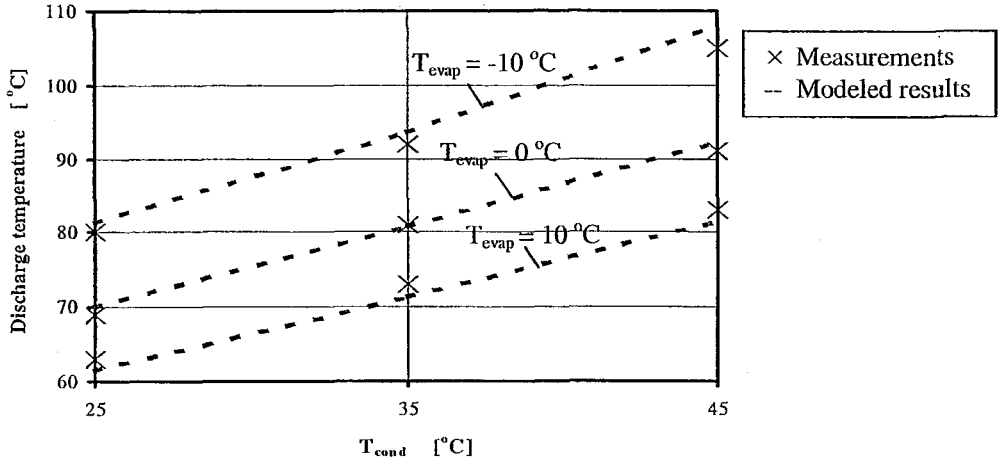

Figure 4 Verification of the discharge temperature

PARAMETRIC STUDY

In order to investigate the compressor's behavior under the variation of different compressor parameters, a parametric study of the scroll compressor was performed. The results can be used to indicate how the compressor design might be altered to achieve better performance.

Variation of the Leakage Gap Size

It has already been mentioned that leakage can account for significant losses in a compressor. In order to investigate how sensitive the compressor's performance with respect to leakage is, computer simulations for different radial and flank leakage gap size were performed. For this purpose, the gap size was specified as a fixed value rather than using the correlation for the gap size as a function of the operating condition. The calculations for different gap sizes were performed for the operating point which is defined by the evaporating temperature of $0^o C$ (corresponding to suction pressure of $497\,kPa$), condensing temperature of $35^o C$ (corresponding to discharge pressure of $1354\,kPa$) and $10^o C$ suction superheat.

The flank leakage gap, δ_f, is calculated using the manufacturer provided correlation and is zero for this specific operating point. The radial leakage gap δ_r calculated using another correlation was used as a standard gap δ_s to evaluate the variations of both the radial and flank leakage gap. The radial and flank leakage gap were varied from 0 to 8 times the standard gap. The calculated mass flow rate as a function of the gap is shown in figure 5.

It can be seen that the mass flow rate decreases linearly with increasing radial/flank leakage gap size. The mass flow rate decreases from $61.05\,kg/h$ at no radial leakage to $47.36\,kg/h$ for the radial leakage gap at 8 times of the standard gap δ_s, corresponding to a loss of volumetric efficiency of 22.42%. The mass flow rate

decreases from 59.47 kg/h at no flank leakage to 53.78 kg/h for the flank leakage gap at 8 times the standard gap δ_s, corresponding to a loss of volumetric efficiency of 9.57%. More importantly, reducing the radial leakage gap size to zero from the current design does not improve the mass flow significantly.

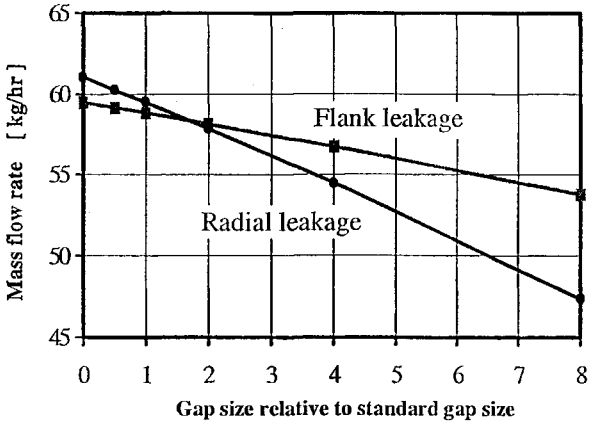

Figure 5 Mass flow rate vs. leakage gap size

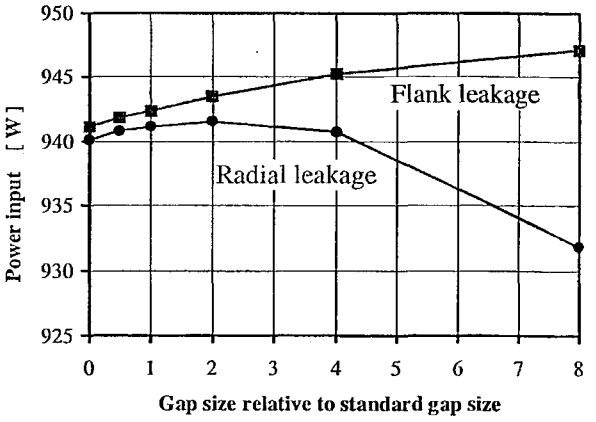

Figure 6 Power input vs. leakage gap size

The power input to the compressor was calculated assuming that the motor-mechanical efficiency $\eta_{motor-mechanical}$ is not influenced by variation of the radial/flank leakage gap, based on the fact that $\eta_{motor-mechanical}$ was defined to cover the motor losses and mechanical losses. The power input as a function of the leakage gap is shown in figure 6. Due to the decreasing mass flow rate, it can be seen that less power input is required to compress the refrigerant from suction to discharge pressures as the radial gap size increases. On first glance this might appear to be an advantageous behavior, since it is desirable to run the compressor with as little power input as possible. However, since the mass flow rate decreases, the cooling effect that can be achieved decreases as well. Since the decrease of the mass flow rate for increasing the flank leakage is not as much as the decrease for increasing the radial leakage, the power input increases as the flank gap size increases.

The overall compressor efficiency is defined as follows:

$$\eta_{compressor} = \frac{\dot{W}_{isentropic}}{P} \tag{19}$$

where the isentropic compression work $\dot{W}_{isentropic}$ can be calculated by

$$\dot{W}_{isentropic} = \frac{\kappa}{\kappa - 1}\frac{P_{suc}}{\rho_{suc}}\left[\left(\frac{P_{dis}}{P_{suc}}\right)^{\frac{\kappa-1}{\kappa}} - 1\right]\dot{m} \tag{20}$$

The calculated overall compressor efficiency as a function of the leakage gap is shown in figure 7. It can be seen that with the increase of the radial and flank leakage gap size, the compressor efficiency decreases from 49.20% to 38.51% and from 47.88% to 43.09%, respectively.

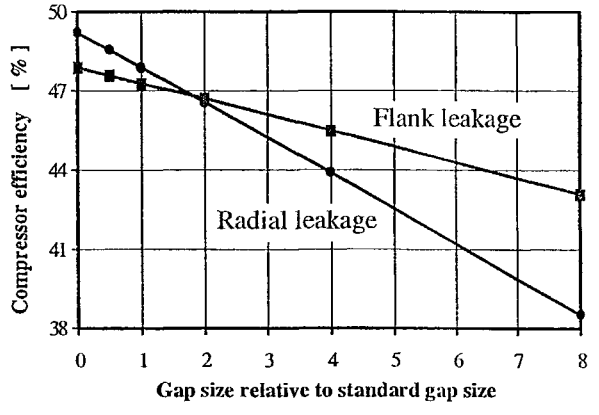

Figure 7 Compressor efficiency vs. leakage gap size

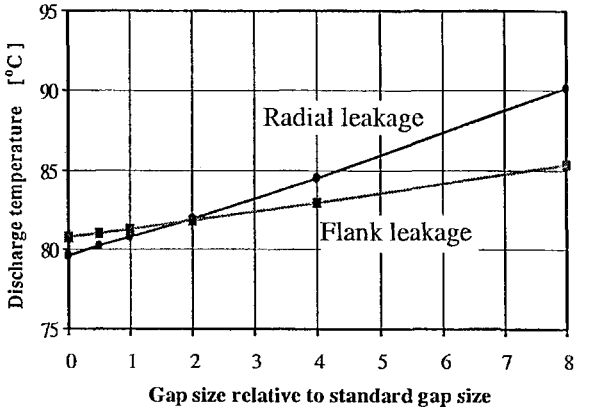

Figure 8 Discharge temperature vs. leakage gap size

The compressor discharge temperature is shown in figure 8 as a function of the leakage gap size. The discharge temperature increases with leakage gap size. This is due to the fact that with increasing the

radial/flank leakage gap size, more refrigerant flows back from the high pressure chamber to the low pressure chamber, which causes more refrigerant to be recompressed and reheated. In addition, the mass flow rate decreases more dramatically with increasing radial leakage gap than with increasing flank leakage gap. Therefore, the energy dissipated in the motor which heats the gas after it is discharged from the pump assembly per unit mass flow rate also increases more with increasing radial leakage gap size. This causes the discharge temperature to increase more for increasing radial leakage, as seen in figure 8.

It can be concluded that the performance of the compressor is more sensitive to the radial leakage gap than to the flank leakage gap. By decreasing the radial/flank leakage gap, the performance can be improved.

Variation of the Heat Transfer Coefficient

Heat transfer between the refrigerant and the scroll wraps/plates during the compression process influences the performance of the compressor. In order to investigate the sensitivity of the compressor's performance with respect to heat transfer, computer simulations for different heat transfer coefficients were performed. For this purpose, a coefficient varying from 0 to 8 was multiplied by the standard heat transfer coefficient h_c which was calculated using the correlation for the spiral heat exchanger as described in Chen et al (2000). The calculations for different heat transfer coefficients were performed for the same operating point as previously defined.

In figure 9, the calculated mass flow rate is shown as a function of the heat transfer coefficient. It decreases from a mass flow rate of $60.19\,kg/h$ with no heat transfer to $56.47\,kg/h$ at 8 times multiplier the standard heat transfer coefficient h_c, which corresponds to a loss of volumetric efficiency of 6.18%. The mass flow rate decreases because with an increase in heat transfer coefficient, the refrigerant in the two suction chambers is heated more by the scroll wraps/plates, which causes the density of the suction refrigerant to be less. Note that reducing the heat transfer (from current design) does not have much effect.

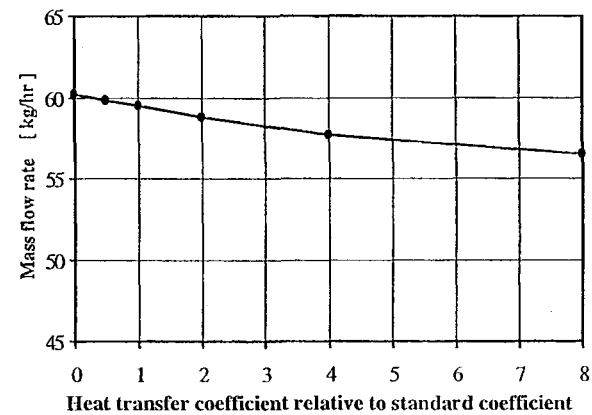

Figure 9 Mass flow rate vs. heat transfer coefficient

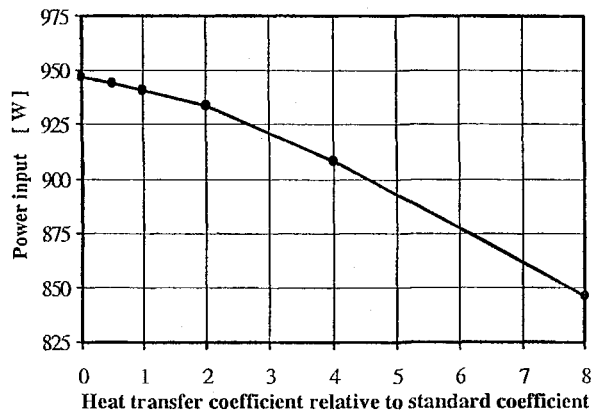

Figure 10 Power input vs. heat transfer coefficient

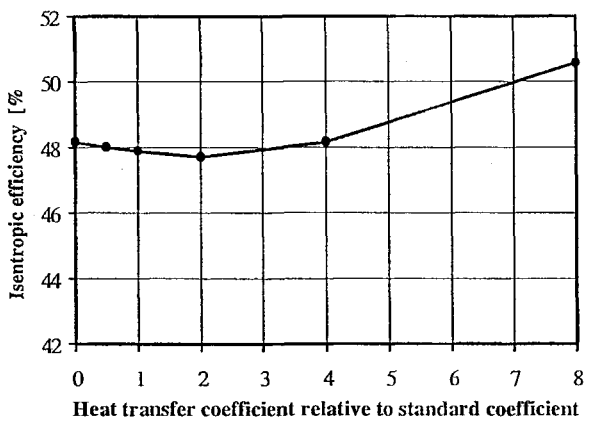

Figure 11 Compressor efficiency vs. heat transfer coefficient

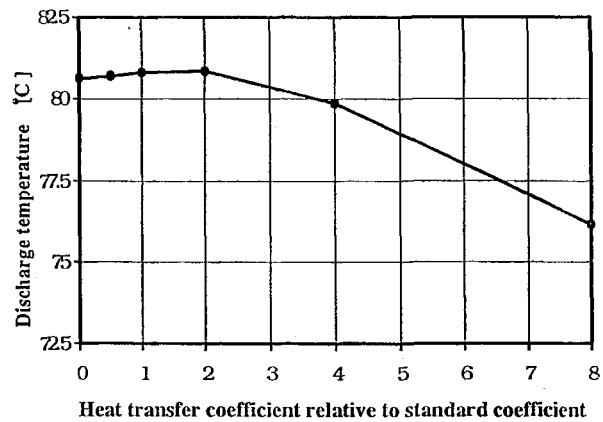

Fig 12 Discharge temperature vs. heat transfer coefficient

The calculated power input, overall compressor efficiency, and discharge temperature as a function of the heat transfer coefficient multiplier are shown in figures 10 to 12. The temperature distribution of the scroll wrap is assumed to be linear. By comparing the temperature of scroll wrap and the refrigerant, it is found that

the temperature of the scroll wrap is always higher than that of the refrigerant in the suction chambers for a full rotation. The temperature of the scroll wrap is higher than that of the refrigerant in the compression chambers for part of the rotation and then becomes lower for the rest of the rotation. The temperature of the scroll wrap is always lower than that of the refrigerant in the discharge chamber for the full rotation. Therefore, with increasing heat transfer coefficient, the refrigerant in the suction chambers is heated more, which causes the mass flow rate to become less. Also, with increasing heat transfer coefficient, the refrigerant in the compression chamber and discharge chamber is cooled more, which causes discharge temperature and compression work/power input to become less.

From the above analysis it can be concluded that with the increases of the heat transfer coefficient, the volumetric efficiency becomes worse while the compressor efficiency becomes better. From figures 9 to 12, it can also be seen that for the variation of the heat transfer coefficient from 0 to 4 times the standard heat transfer coefficient, the slope of the performance of the compressor is rather small, which implies that the performance of the compressor is not very sensitive to the heat transfer coefficient for this range.

Variation of the Scroll Geometry

The performance of a scroll compressor is influenced by its geometrical design. In order to investigate the compressor's performance under geometrical variation, six different shapes were chosen so that the volume of the suction chambers and compression chambers remained constant. This was achieved by varying the radius of the involute's basic circle from 0.5 to 2.5 times the original design radius r_b and by adjusting the scroll height to give constant volumes.

In figure 13, the calculated mass flow rate is shown as a function of the radius of the basic circle. It decreases from a mass flow rate of $60.48\,kg/h$ at 0.5 times the original radius r_b to $57.05\,kg/h$ at 2.5 times r_b, which corresponds to a decrease of volumetric efficiency of 5.61%. The mass flow rate decreases because with the increased radius of the basic circle, the area of the passage of the radial leakage flow increases, which causes the mass flow rate to decrease.

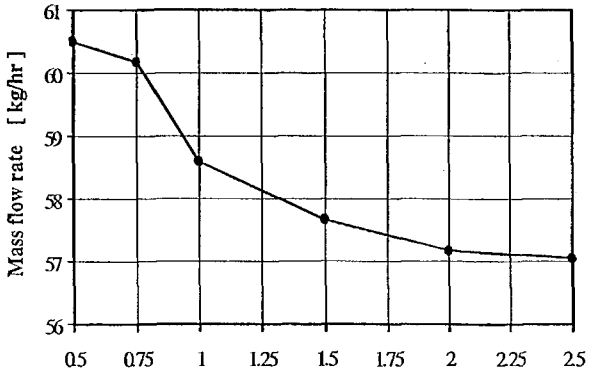

Figure 13 Mass flow rate vs. radius of the basic circle

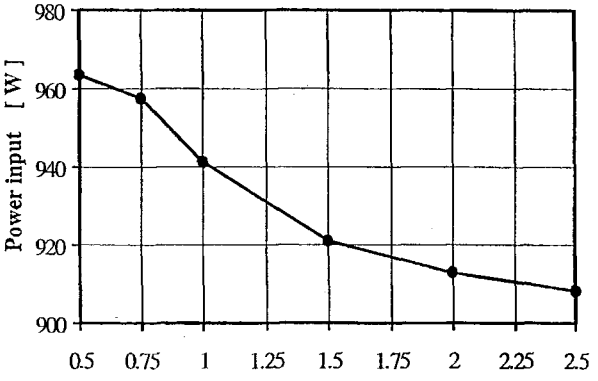

Figure 14 Power input vs. radius of the basic circle

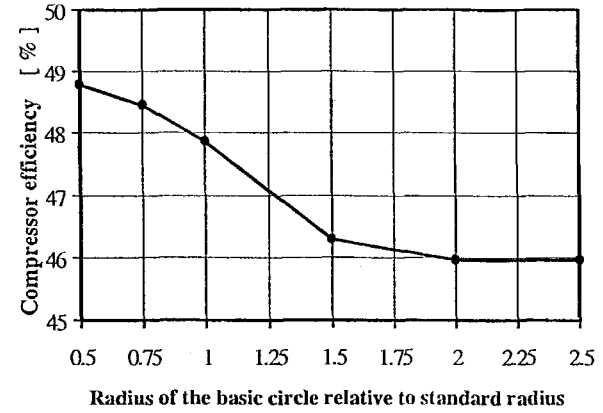

Figure 15 Compressor efficiency vs. radius of the basic circle

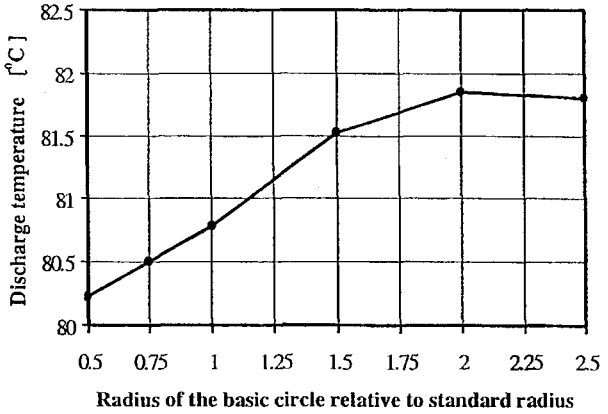

Figure 16 Discharge temperature vs. radius of the basic circle

The calculated power input, overall compressor efficiency and discharge temperature as a function of the radius of the basic circle are shown in figure 14 to 16. Power input decreases as a function of the radius of the basic circle due to the decreased mass flow rate. Due to more and more radial leakage, the compressor efficiency decreases and the discharge temperature increases.

It can also be found that when the radius decreases to 0.5 times of the original designed radius, the performance of the compressor becomes less and less sensitive to the radius change. Therefore, by decreasing the radius of the basic circle, the compressor's performance can be improved to a certain level.

CONCLUSIONS AND RECOMMENDATIONS

Overall energy balances for the various compressor elements were established to model the heat transfer between each of the compressor elements. Together with a detailed compression process model, a comprehensive compressor simulation model was developed that predicts the power input to the compressor, the discharge temperature, and the mass flow rate. In order to validate the model, a compressor load stand was built. The load stand is a hot-gas bypass type, where part of the refrigerant goes through a phase change in a condenser while the other part of the flow bypasses the condenser and is routed back to the suction inlet via an expansion device. The load stand was found very useful to produce defined operating conditions for the compressor such as suction temperature, suction pressure and discharge pressure. Through model validation, it was found that the compressor model can predict the mass flow rate, the power input and the discharge temperature very well. A parametric study of the compressor was performed using the model. The influence of radial and flank leakage and heat transfer between the refrigerant and the scroll wraps/plates on the compressor's performance was investigated. The influence of these effects was also studied for scroll designs with geometrical variations. From these studies the following conclusions can be drawn:

1. Leakage can have a tremendous effect on the compressor's performance. Due to leakage, the volumetric efficiency decreases. For the same gap size, however, radial leakage decreases the volumetric efficiency far more than flank leakage, which is due to a bigger cross sectional flow area. It can be seen that for the current design, the effect of leakage is small.
2. Heat transfer between the refrigerant and the scroll wraps/plates decreases the compression work due to the cooling effect of the refrigerant in the compression and discharge chamber, leading to a lower discharge temperature from the pump assembly. Due to suction gas heating in the suction chamber, heat transfer into the refrigerant reduces the volumetric efficiency, since the suction gas density is decreased. It can also be seen that the effect of heat transfer is small for the current design.
3. Scroll geometry influences the performance of the scroll compressor. For the same suction and compression volume, within a certain limit, a smaller radius of the basic circle results in improved performance.

REFERENCES

[1] Yunus A. Cengel and Michael A. Boles *Thermodynamics: an Engineering Approach.* McGraw-Hill, Inc., New York, 1989.

[2] Y. Chen, N. Halm, E. Groll and J. Braun. A Comprehensive Model of Scroll Compressor Part I: Compression Process Modeling, *Proceedings of International Compressor Engineering Conference at Purdue*, 2000.

[3] S.D. Conte and C. DeBoor. *Elementary numerical analysis.* McGraw Hill, Inc., New York, 1980.

[4] M. Hayano et al, An analysis of losses in scroll compressors, *Proceedings of International Compressor Engineering Conference at Purdue*, 1988

[5] Nils P. Halm. Mathematical modeling of scroll compressors. *Master thesis of Herrick lab, School of Mechanical Engineering, Purdue University*, 1997.

NOMENCLATURE

Symbol	Description
h_c	Standard heat transfer coefficient
h_{gas}	Specific enthalpy of the refrigerant as discharged from compressor
h_{dis}	Average specific enthalpy of gas as discharged from pump assembly
h_{suc}	Specific enthalpy of the refrigerant at the suction of the compressor
κ	Specific heat ratio of the refrigerant
$\dot{m}$	Mass flow rate of the refrigerant
P	Power input to the compressor
P_{cond}	Condensing pressure

Symbol	Description
P_{dis}	Discharge pressure of the refrigerant
P_{evap}	Evaporating pressure
P_{suc}	Suction pressure of the refrigerant
P_{suc}	Suction pressure of the refrigerant
$\dot{Q}_{ambient}$	Heat transfer rate to the ambient through the compressor shell
$\dot{Q}_{average\_alum}$	Average heat transfer rate from the refrigerant to the aluminum scroll
$\dot{Q}_{average\_steel}$	Average heat transfer rate from the refrigerant to the steel scroll
$\dot{Q}_{friction}$	Heat transfer rate to the compressor element due to the frictional losses
$\dot{Q}_{friction\_steel}$	Heat transfer rate to the steel scroll due to the frictional losses
$\dot{Q}_{friction\_alum}$	Heat transfer rate to the aluminum scroll due to the frictional losses
$\dot{Q}_{friction\_rot}$	Heat transfer rate to the motor rotor due to the frictional losses
$\dot{Q}_{friction\_stat}$	Heat transfer rate to the motor stator due to the frictional losses
$\dot{Q}_{friction\_oil}$	Heat transfer rate to the oil due to the frictional losses
$\dot{Q}_{loss}$	Power input losses including motor and frictional losses
$\dot{Q}_{motor}$	Heat transfer rate to the motor due to motor losses
$\dot{Q}_{pipe1}$	Heat transfer rate from the refrigerant to the suction pipe 1
$\dot{Q}_{pipe2}$	Heat transfer rate from the refrigerant to the suction pipe 2
r_b	Radius of the basic circle of the scroll
R	Thermal resistance between two compressor elements

Symbol	Description
T_{dis}	Temperature of the refrigerant at the discharge port of the scroll
T_{amb}	Temperature of the ambient
T_{alum}	Average temperature of aluminum scroll
T_{cond}	Condensing temperature of the refrigerant
T_{evap}	Evaporating temperature of the refrigerant
T_{gas}	Temperature of the refrigerant discharged from the compressor
T_{oil}	Temperature of the compressor oil
T_{pipe1}	Temperature of the suction pipe on the outside of the compressor
T_{pipe2}	Temperature of the suction pipe on the outside of the compressor
T_{ref}	Temperature of the refrigerant as a function of the orbiting angle
T_{rot}	Temperature of the motor rotor
T_{stat}	Temperature of the motor stator
T_{shell}	Temperature of the compressor shell
T_{steel}	Average temperature of steel scroll
T_{suc}	Suction temperature of the refrigerant
$\dot{W}_{compression}$	Real compression work (fluid work) to the refrigerant
$\dot{W}_{isentropic}$	Isentropic work to the refrigerant
ρ_{suc}	Suction density of the refrigerant
δ_f	Flank leakage gap
δ_r	Radial leakage gap
δ_s	Standard leakage gap
$\eta_{isentropic}$	Isentropic efficiency of the compressor
$\eta_{compressor}$	Overall compressor efficiency
$\eta_{motor-mechanical}$	Efficiency which covers both motor and mechanical losses